HEATING RATE LIMITED KINETICS OF CRYSTALLIZATION OF FINEMET+NI AMORPHOUS RIBBONS

E. Illeková, P. Duhaj
Institute of Physics, Slovak Academy of Sciences, Dúbravská cesta 9, SK-84228 Bratislava, Slovak Republic

Received 14 April 2000, accepted 12 June 2000

The crystallization kinetics of the $Fe_{53.5}Ni_{20}Cu_1Nb_3Si_{13.5}B_9$ glassy ribbon was investigated by differential scanning calorimetry. The phase identification in the linearly heated samples was performed by X-ray diffraction. The linear heating thermograms indicate an anomalous heating rate dependence. It was found that both kinetics and mechanisms of glass crystallization suddenly change when the heating rate falls below its critical value, w = 20 K min^{-1}. The crystallization proceeds as a two step (R1 and R2) transformation using small heating rates $w < 20$ K min^{-1}. The activation energies E_1^* = 302 kJ mol^{-1} and E_2^* = 345 kJ mol^{-1} indicate atomic transport mechanisms. The ordered Fe_3Si and $Fe_3NiSi_{1.5}$ nanocrystalline phases crystallize separately in the R1 and R2 steps. In the same material both phases crystallize simultaneously in one crystallization step (R3) by the viscous flow mechanism (E_3^* = 718 kJ mol^{-1}) at higher heating rates, $w \geq 20$ K min^{-1}. The DSC experiments gave evidence of the diffusion of nickel, which starts before the crystallization and controls an alternative crystalline phase nucleation.

PACS: 81.05.Kf, 82.20.Mj, 82.60.Nh, 64.70.Kb, 81.40.-z, 81.40.Ef, 81.05.Bx, 81.05.Ys,

The crystallization kinetics of Fe-B-based and Fe-Si-B-based amorphous alloys indicates usually more-or-less modified Johnson-Mehl-Avrami-type (JMA) nucleation-and-growth-like processes [1, 2]. Contrarily, $Fe_{73.5}Cu_1Nb_3Si_{13.5}B_9$ (so called FINEMET) is characterized by the normal-grain-growth-like (GG) kinetics which leads to the nanocrystalline structure formation [3, 4]. Irrespective of the type, the crystallization of these metallic alloys is always considered and viewed as a phase transformation with a well-defined kinetics. It means that neither the type of the kinetic equation nor the kinetic parameters of the elementary microprocesses are dependent on either the temperature regime (heating rate, w, or isothermal annealing temperature, T_a) or the degree of conversion, α, of the sample during the crystallization. In this letter, we present a glassy material where, for the first time, this is not the case. The composition of the glass differs from FINEMET because it contains 20 at.% of Ni, which replaces part of the Fe. The differential scanning calorimetry (DSC) measurements were performed at various heating rates, w, to investigate the kinetics of nanocrystallization in this glass. It was found that the FM+20Ni sample exhibits two slight exothermic crystallization reactions between 770 K and 970 K at the heating rates up to w = 10 K min^{-1} whereas only one fast crystallization step occurs at heating rates

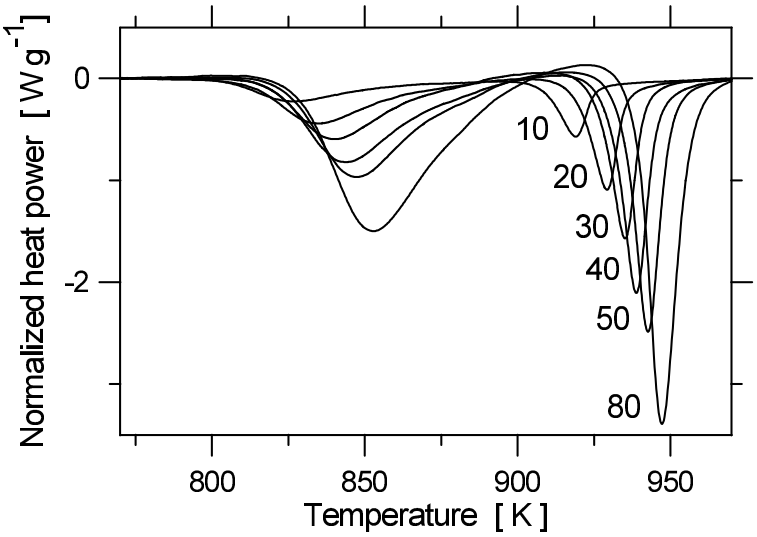

Fig. 1. DSC linear-heating curves of the as-quenched $Fe_{63.5}Ni_{10}Cu_1Nb_3Si_{13.5}B_9$ (FM+10Ni) ribbon taken at various heating rates. The heating rate is the parameter.

$w \geq 20$ K min^{-1}. This unexpected change in the DSC thermogram might be explained by superposition of two crystallization steps with extremely different activation energies or as a general consequence of another processes (particular diffusion of Ni) controlling spatial fluctuations in the amorphous matrix impurities, composition or ordering before the onset of the crystallization. This question is going to be answered.

The master alloys were prepared from the constituent elements of at least 99.5% purity. The $Fe_{73.5-x}Ni_xCu_1Nb_3Si_{13.5}B_9$ glassy ribbons, (x = 0 - 50), 10 mm wide and 30 μm thick, were prepared by the planar-flow casting method. Chemical analysis of the ribbons was performed by inductively coupled plasma spectroscopy. The linear-heating crystallization measurements on the as-cast samples were performed in the Perkin-Elmer DSC7 instrument using w of 5 – 80 K min^{-1}. N_2 gas flow for the ambient atmosphere was utilized. The absolute temperature (error less than 0.05%) and the enthalpy (error less than 2%) of the DSC instrument were calibrated for all heating rates.

Figure 1 shows a typical set of linear heating DSC thermograms of the FM+10Ni sample. A two-step crystallization process occurs between 770 and 970 K. In accordance with the presumption about thermal activation of crystallization controlling processes, both exothermal peaks are heating rate dependent. The first exotherm maximum and the position of the second peak are significantly shifted to higher temperatures with increasing w. All FM+xNi samples behave similarly except FM+20Ni.

Figure 2 shows the linear heating DSC thermograms of the FM+20Ni sample. Again, two crystallization peaks (R1 ands R2) occur between 770 and 970 K at heating rates $w \leq 10$ K min^{-1}. However, at w = 20 K min^{-1} two new crystallization exothermal events (R3 and R4) appear in the same temperature interval. The first of them (R3) has the shoulders at both sides likely coming from the previous two ones (R1 and R2). At higher heating rates, only one massive

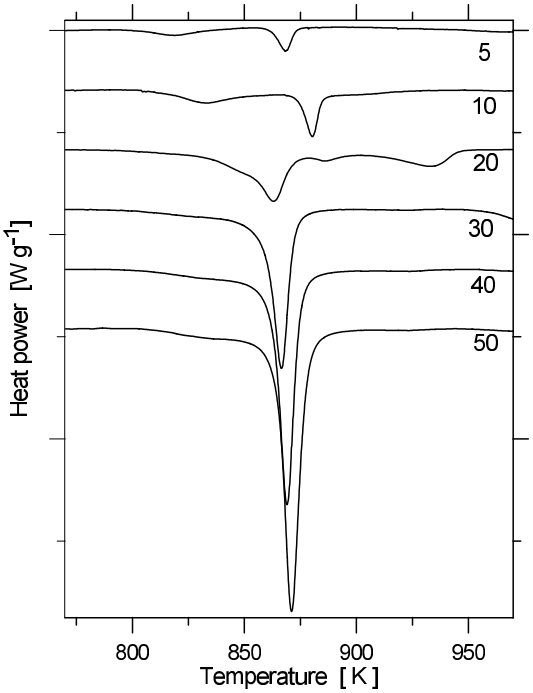

Fig. 2. DSC linear-heating curves of the as-quenched $Fe_{53.5}Ni_{20}Cu_1Nb_3Si_{13.5}B_9$ (FM+20Ni) ribbon taken at various heating rates. The heating rate is the parameter.

crystallization exotherm (R3) can be seen while R4 crystallization step is shifted above 970 K. The crystallization enthalpy of the R1 peak $\Delta H_1 \sim 38$ J g^{-1} at w = 5 K min^{-1} significantly decreases and that of the R2 peak $\Delta H_2 \sim 42$ J g^{-1} increases with increasing w. At w = 30 K min^{-1}, the crystallization enthalpy of the R3 peak is $\Delta H_3 \sim 73$ J g^{-1} and this quantity slightly increases with increasing w. Such a sudden change of the crystallization kinetics of a metallic glass after a moderate increase of heating rate is observed for the first time. Few indications are known about the crucial annealing temperature, T_a, dependence on the grain size in different alloy systems, namely if $T_a \sim 0.5T_m$ (T_m is the melting temperature) [5]. Kulik reported in [6] about the change of the size, morphology, kinetics and composition at the first step of isothermal nanocrystallization in a FeCuSiB glass by changing T_a by more than 105 K. However, no limiting heat-treatment parameters, T_a or w, affecting the kinetics, mechanism or chemical composition of the crystallizing phases in the case of metallic glasses have been observed yet.

Following the theory [7], $dH/dt = m\Delta H_{tr} w d\alpha/dT$, so that the DSC signal dH/dt is proportional to w. Furthermore, the temperature of the transformation peak maximum, T_p, increases with increasing w in such a way that the slope of the $\ln(w/T_p^2)$ versus $1/T_p$ linear plot gives the activation energy of the transformation [8]. The heating rate dependence of the thermograms in Fig. 2 does not fulfill any of these axioms. In all $w \geq 20$ K min^{-1} thermograms, the R3 peak has the activation energy E_3^* = 718 $\pm$ 25 kJ mol^{-1} evidently different from those of R1 or R2 peaks, namely $E_1^* \sim 302$ kJ mol^{-1} and $E_2^* \sim 345$ kJ mol^{-1} as can be seen in Fig. 3. The R4

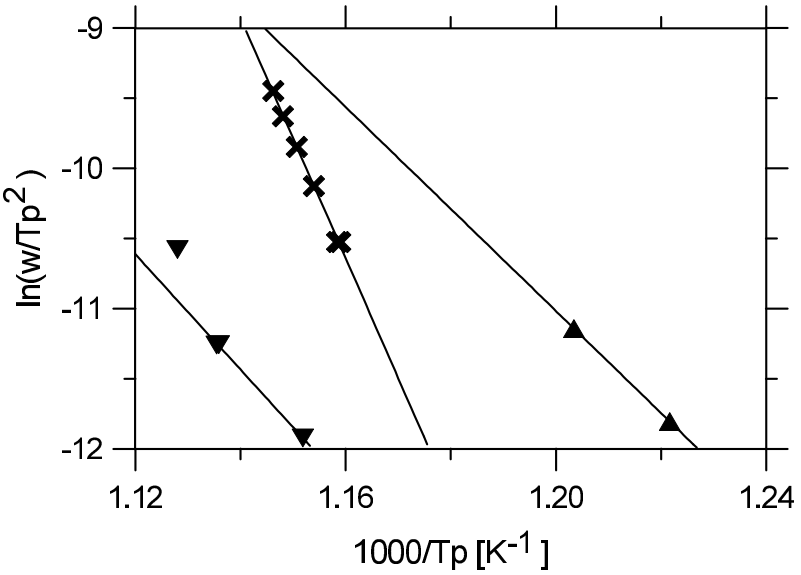

Fig. 3. Kissinger plots [8] of the heating rate shift in the DSC peak temperature for the $Fe_{53.5}Ni_{20}Cu_1Nb_3Si_{13.5}B_9$ glassy ribbon. The activation energies for the R1 (△), R2 (▽) and R3 (×) peaks are estimated as $E_1^* \sim 302$, $E_2^* \sim 345$ and $E_3^* = 718 \pm 25$ kJ (g atom)$^{-1}$, respectively.

peak (ΔH_4 = 18 J g^{-1}) in the w = 20 K min^{-1} thermogram is smaller than any of the peaks in the w = 10 K min^{-1} thermogram which indicates a change in the mass, m and/or ΔH_{tr} of the crystallizing product in the sample.

In order to receive further experimental evidence whether the extraordinary heating rate dependence of the DSC peaks in Fig. 2 is correlated with the change of the kinetics of formation of the nanocrystalline phases in the amorphous system, the kinetic exponents were determined and tested. Figure 4 shows the Suriñach representation [9] of the FM+20Ni DSC crystallization peaks. All measured DSC peaks from Fig. 2 were used. In contrast to the GG-like kinetics of the main nanotransformation peak in both FINEMET [3, 4] and FM+10Ni samples [10], the JMA-like kinetics of the R1, R2 and R3 peaks is found in the alloy with 20 at.% of Ni. In the first crystallization step, R1, the JMA exponent [11] n_1 = 2 and in the second crystallization step, R2, n_2 = 4 at small heating rates. Both exponents quickly decrease above 30 % and 40 % degree of conversion, respectively. Contrary to R1 and R2 peaks, every R3 peak (measured at any $w > 20$K min^{-1}) follows one characteristic master curve. An additional process always contributes to the kinetics at the beginning of the main R3 process (see also Fig. 2). The homogeneous nucleation and the three-dimensional crystal growth mechanisms with n_3 = 4 unambiguously characterize the central part of this peak for 30 to 70 % degree of conversion. Afterwards, both nucleation and growth processes die out. In spite of the fact that the complete R4 DSC peak was observable only at the heating rates from 15 to 25 K min^{-1}, incontestably this transformation step is controlled by the long-range diffusion of participating particles.

Evolution of the structure and the phase identification in the samples heated linearly were performed by X-ray diffraction. The samples were heat-treated using heating rates 2 and 40 K

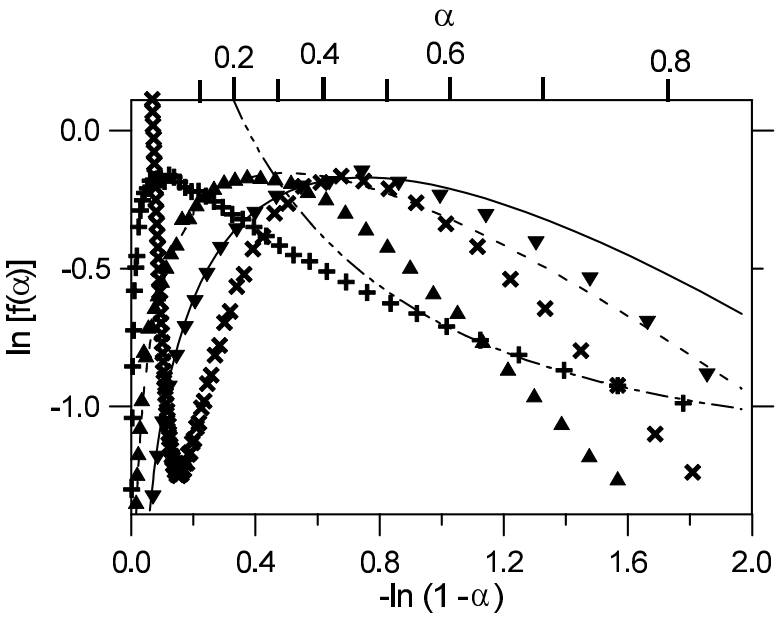

Fig. 4. Suriñach plots [9] for R1, R2, R3 and R4 crystallization peaks of the $Fe_{53.5}Ni_{20}Cu_1Nb_3Si_{13.5}B_9$ glassy ribbon taken at linear heating and the theoretical curves obtained for the JMA kinetic equation with the exponents n_1 = 2 (- - - - -) and $n_2 = n_3$ = 4 (———) in the early stages of R1, R2 and in the central part of R3 peak, respectively and for the one dimensional long-range diffusion equation in the case of R4 transformation (–...–...). The lines are the theoretical curves. Symbols are the experimental data for R1 (△) and R2 (▽) at w = 5 K min^{-1} and for R3 (×) at w = 50 K min^{-1} and R4 (+) at w = 20 K min^{-1}.

min^{-1} in a vacuum furnace at the pressure of 10^{-3} Pa. The X-ray measurements were performed using the CuK_α radiation and a graphite monochromator in the diffracted beam. Up to the onset of R1 or R3 transitions, the diffraction patterns did not indicate any crystalline phases (Fig. 5a is given as an example). The diffraction patterns f or the partially or fully crystalline samples depend on the preceding heating rate of the sample. In the case of small heating rates, as it was the case for w = 2 K min^{-1}, further increase of temperature results into the formation of nanocrystalline [12] Fe_3Si phase with DO_3 structure type. This phase is the only phase formed in this alloy up to the upper limit of R1 peak (Fig. 5b). Additional lines corresponding to the tetragonal $Fe_3NiSi_{1.5}$ phase with the lattice parameters a = b = 0.8325 nm, c = 0.903 nm appear after the onset of R2 transformation. Linear heating to the temperatures corresponding to the upper limit of R2 peak gave rise to a more complex pattern which was still dominated by ordered Fe_3Si and $Fe_3NiSi_{1.5}$. The borides like orthorhombic Ni_3B and orthorhombic Fe_3B were present, too. Moreover, several reflections which could not be indexed according to any known binary or ternary phases in the Fe-Ni-Si or Ni-Si-B systems were found to be present (Fig. 5c). In the case of higher heating rates, as it was the case for w =40 K min^{-1}, ordered Fe_3Si and $Fe_3NiSi_{1.5}$ nanoparticles are undoubtedly formed from the beginning of the main R3 crystallization step. In the maximum of the R3 transition, orthorhombic Ni_3B reflections and weak orthorhombic Fe_3B ones were also registered. At 873 K, the content of Ni_3B phase culminates (Fig. 5d) and at

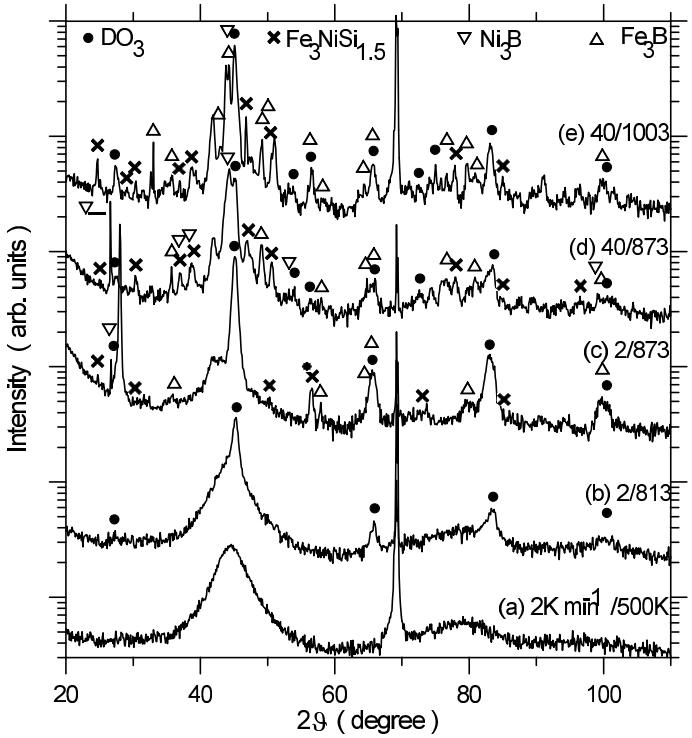

Fig. 5. X-ray diffraction patterns taken on the $Fe_{53.5}Ni_{20}Cu_1Nb_3Si_{13.5}B_9$ glassy ribbon heat-treated by linear heating to various final temperatures. The heating rate and the final temperature are the parameters.

higher temperatures the intensity of Ni_3B reflections diminishes in favour of the Fe_3B ones. At the maximum of the R4 transition, no Ni_3B reflections were observed (Fig. 5e). The appearance of borides already in the main R3 nanotransformation step is not surprising in the case of nickel containing alloys. They were already observed near 780 K in Ni-Si-B glass [13], above 750 K in Fe-Ni-Si-B amorphous ribbons [14] and their presence was also concluded in the FM+20Ni alloy at 823 K [15].

In [14, 16], the two step crystallization of the glassy $Fe_{58}Ni_{20}Si_9B_{19}$ alloy was investigated both isothermally and upon a linear heating. In this sample, a two step crystallization at $\sim$ 700 K and above $\sim$ 750 K was observed. It was found that as the temperature of isothermal heat-treatment decreases below 600K, the activation energy responsible for the crystallization decreases by more than 50 %. In this case, the range of a "low temperature" crystallization was established. It was characterized by a reduced activation energy of the precrystallization processes $E_\tau^* < 154$ kJ mol^{-1}, no new phase nucleation and only a diffusion controlled growth of crystals. At higher temperatures, the activation energy of structural relaxation (314 kJ mol^{-1}) was equal to that of the process responsible for crystallization, E_τ^* = 301 kJ mol^{-1}. No heating rate influences were reported. These results brought two remarkable conclusions which support our observations. Firstly, the JMA type crystallization may proceed also at 100 - 150 K below the onset temperature of the linear heating crystallization. Secondly, the precrystallization processes

in the case of the Ni containing Fe-Si-B glasses significantly influence the mechanisms of the crystallization.

In the case of Metglas 2826 ($Fe_{40}Ni_{40}P_{14}B_6$), Tiwari [17] determined the activation energies for growth, nucleation and the total process of eutectic type crystallization employing transmission microscope technique (TEM) as E_G^* = 345 kJ mol^{-1}, E_N^* = 800 kJ mol^{-1} and E_{total}^* = 440 kJ mol^{-1}, respectively. The difference in E_G^* and E_N^* indicates that the atomic transport mechanisms in these two microprocesses are not the same in this glassforming system. These observations also lead to the conclusion that the process of nucleation is related to the viscous flow (its activation energy is E_η^* = 620 kJ mol^{-1} [17]) while the growth process in this alloy is governed by the short-range diffusion across the crystal-glass interface. Our E_1^* = 302 kJ mol^{-1} and E_2^* = 345 kJ mol^{-1} values correlate well with E_G^* = 345 kJ mol^{-1} from [17]. Also E_3^* = 718 kJ mol^{-1} correlates with E_N^* = 800 kJ mol^{-1} and E_η^* = 620 kJ mol^{-1} from [17] in spite of a principal difference in the size of crystallized grains.

In [12], the influence of Ni (up to 40 at.%) on the isothermal formation of the nanocrystalline phases in $Fe_{(73.5-x)}Ni_xCu_1Nb_3Si_{13.5}B_9$ amorphous ribbons was studied by TEM, electron diffraction, X-ray diffraction and Mössbauer spectroscopy. It was shown that after annealing at temperatures 773 - 873 K, the stability of the nanocrystalline ordered Fe_3Si phase rapidly decreases with increasing Ni content. The nanocrystalline phase gradually decomposes, the grains increase in size and a new tetragonal phase $Fe_3NiSi_{1.5}$ with a = b = 0.8325 nm, c = 0.903 nm can be observed. In the alloys with Ni content above 20 at.%, already an annealing at 773 K leads to the formation of the Fe_3Si and $Fe_3NiSi_{1.5}$ phases. The observations in [12] are analogous to our results. However, both above mentioned [14, 16, 17] and our results give serious indications that the isothermal crystallization path need not be equivalent to the linear heating one in the case of the FM+20Ni sample. Most likely, the crystallization processes, which proceed isothermally at any T_a of 773 - 873 K (after placing the sample into the heated to T_a furnace) take place in the same way as in the case of higher heating rate. Next, we conclude that it is not the absolute value of T_a but the time t_0, during which the sample is exposed to the temperatures significantly lower than the crystallization temperatures at linear heating, which controls the crystallization in these samples. During this time, the Fe_3Si-like or the $Fe_3NiSi_{1.5}$-like medium-range order at the scale of embryos might be formed. Afterwards, in the crystallization temperature intervals, the ordered Fe_3Si and $Fe_3NiSi_{1.5}$ phases can nucleate and grow by a short-range diffusion through the crystal-glass interface. If the medium-range order is not formed, the crystallization of both phases proceeds simultaneously by the viscous flow.

In this letter, we gave experimental indications of the existence of the anomalous heating rate dependence of the crystallization in metallic glasses kinetics (characterized by the DSC peaks). In the $Fe_{53.5}Ni_{20}Cu_1Nb_3Si_{13.5}B_9$ glassy ribbon, the ordered Fe_3Si and $Fe_3NiSi_{1.5}$ nanocrystalline phases crystallize separately in the R1 and R2 crystallization steps at small heating rates. In this case, the diffusion of nickel, proceeding already at lower temperatures before the crystallization, results into a medium-range ordering. Afterwards, nucleation and particularly growth of the above-mentioned phases are governed just by adequate glass-crystal interface oversteps. The activation energies E_1^* = 302 kJ mol^{-1} and E_2^* = 345 kJ mol^{-1} indicate the atomic transport mechanisms. Both crystallization steps saturate quickly, n_1 decreasing from 2 to < 1 and n_2 from 4 to 1.5. The ordered Fe_3Si and $Fe_3NiSi_{1.5}$ phases crystallize simultaneously in one crystallization step (R3) by the viscous flow mechanism at higher heating rates, $w \geq 20$ K min^{-1}. The devitrification proceeds by the JMA nucleation-and-growth kinetics with n_3 = 4 and E_3^* =

718 kJ mol^{-1}. Subsequently, also the Ni_3B and first Fe_3B borides are formed. At higher temperatures Ni_3B is destabilized and transforms into Fe_3B by the long-range diffusion of nickel in the R4 transformation step.

Our interpretation of the crystallization anomalies of the FM+20Ni glassy ribbon is based on the correlation between the change of the atomic transport mechanism (from the short-range diffusion to the viscous flow) and kinetics of the formation of two alternative crystalline phases (the change in E^* and n). We conclude that the diffusion of Ni is the controlling factor and that the prenucleation and nucleation are the controlling processes in the alternative crystalline phase (the ordered Fe_3Si and $Fe_3NiSi_{1.5}$) formation.

Acknowledgement The authors would like to thank Dr P. Švec for the X-ray diffraction patterns. This work was supported by the Grant Agency for Science of Slovakia under the grant No. 2/6064/99.

References

[1] A.L. Greer: *Acta Metall.* **30** (1982) 171

[2] E. Illeková, I. Maťko and P. Duhaj: *J. Mater. Sci.* **32** (1997) 4645

[3] E. Illeková, K. Czomorová, F.A. Kuhnast and J.M. Fiorani: *Mater. Sci. Eng. A* **205** (1996) 166

[4] N. Lecaude and J.C. Perron: *Materials Science Forum* **269-272** (1998) 713

[5] K. Lu: *Mat. Sci. Eng. R* **16** (1996) 161

[6] T. Kulik: *Materials Science Forum* **269-272** (1998) 707

[7] E. Illeková, B. Aba and F.A. Kuhnast: *Thermochimica Acta* **195** (1992) 195

[8] H.E. Kissinger: *Annal. Chem.* **29** (1957) 1702

[9] S. Suriñach, M.D. Baro, M.T. Clavaguera-Mora and N. Clavaguera: *J. Non-Crystalline Solids* **58** (1983) 209

[10] E. Illeková: unpublished data

[11] J.W. Christian: *The Theory of Transformations in Metals and Alloys*, Pergamon, Oxford, 1975

[12] P. Švec and P. Duhaj: *Mater. Sci. Eng.*, in press

[13] S. Stolen: *Journal of Alloys and Compounds* **204** (1994) 47

[14] T.V. Larionova, O.V. Tolochko and A.S. Zhuravlev: *Glass Physics and Chemistry* **21** (1995) 297

[15] P. Vojtaník, E. Komová, P. Petrovič, R. Varga, H. Sassik and R. Grössinger: *Acta Phys. Slov.* **48** (1998) 719

[16] T.V. Larionova, O.V. Tolochko, N.O. Gonchukova and E.V.Novikov: *Glass Physics and Chemistry* **22** (1996) 248

[17] R.S. Tiwari: *J. Non-Crystalline Solids* **83** (1986) 126